General Features and Principles of EPR Nuclear Reactor Operation: A Design and Thermal-hydraulic Calculation Study

Atilla Cakir, Faisal Ahmed Moshiur

[a] $KTH, EMINE$

April 3, 2023

Abstract

This report describes the general features and principles of an EPR nuclear reactor operation. The project consists of six tasks, the first three requiring literature studies, while the last three require calculations to determine the basic design parameters of the reactor core. The tasks include a general design specification of the nuclear power plant, operational principles of the EPR, safety features of the power plant, calculation of selected core parameters, calculation of critical heat flux (CHF) margins in a hot channel, and calculation of the maximum cladding and fuel pellet temperature. The results of the calculations are presented in plots and single parameter values.

1 Introduction

The EPR is a third-generation pressurized water reactor, developed primarily by Électricité de France (EDF) and Framatome (part of AREVA between 2001 and 2017) in France and Siemens in Germany. Initially known as the European pressurized reactor in Europe and the evolutionary power reactor internationally, it is now commonly known as EPR.

The report aims to provide an overview of EPR in the context of the UK EPR, an evolutionary four-loop pressurized water reactor (PWR) developed by EDF and AREVA. The reactor design draws maximum benefits from the operational experience of the French and German fleets and is claimed to meet the Franco-German technical guidelines developed between 1993 and 2000. The report discusses the general features and principles of the EPR operation, including the reactor core design, fuel assembly, reactor coolant system, safety features, and compliance with the European Utility Requirements [9].

2 Design (UK EPR)

The EPR design strives to enhance safety and reduce core damage frequency and releases of radioactivity. Its standardized components and KONVOI design ensure high availability and economic viability. Currently under construction in several countries, the EPR is a four-loop PWR that uses regular water to cool the reactor core by slowing down neutrons to maintain the nuclear chain reaction. The heated water then generates steam that drives the turbine to produce electricity, and the steam is condensed and reused. The design also integrates the

human factor to prevent human error in EPR operation and reduces the risk of beyond-design accident sequences [9].

Pressurized water reactors (PWRs) use regular water to remove heat from the reactor core's nuclear fission process. The water slows down the neutrons to maintain the nuclear chain reaction. The heated water is then transferred to the turbine via steam generators to produce electricity. Electrically powered pumps pump the primary cooling water through the reactor core and steam generators in four loops. The steam generated in the secondary circuit drives the turbine, generating electricity, and the steam is condensed and reused. The pressure and temperature of the cooling water keep it in a liquid state, and a pressurizer controls the pressure in the reactor cooling system.

The French N4 reactor is a pressurized water reactor (PWR) designed and built by Areva NP (now Framatome) in the early 2000s. It has a thermal power output of 1450 MW and a net electrical output of 1300 MW. The N4 is notable for using a 17×17 fuel assembly design, allowing for a higher fuel burnup and lower fuel cycle costs than earlier 14x14 designs. The N4 uses a digital instrumentation and control (I&C) system, improving operational efficiency and safety [9].

The German Konvoi series, also PWRs, were built by Siemens and later Areva NP in the 1980s and 1990s. They have a thermal power output of 1300 to 1400 MW and a net electrical output of $1200 - 1300$ MW. The Konvoi reactors also use a 17×17 fuel assembly design and have a similar digital I&C system as the N4 [9].

In comparison, the EPR (European Pressurized Reactor) is a newer generation PWR that was designed by Areva (now Framatome) and Siemens (now Kraftwerk Union) in the late 1990s. It has a 4000 MW thermal power output and a net electrical output of 1600 MW. The EPR uses a more advanced fuel assembly design, known as the Optimized ZIRLO, which allows for even higher fuel burnup and longer fuel cycle times. The EPR has a fully digital I&C system, further improving operational efficiency and safety [9].

Another important parameter to consider is safety features. The EPR has a passive safety system, the core catcher, designed to capture and contain molten core material in a severe accident. This is in addition to other passive and active safety systems already present in the N4 and Konvoi designs. The EPR also has a double containment building, which provides an extra layer of protection against releasing radioactive material [9].

Regarding construction cost and time, the EPR has faced some challenges. The first two EPRs built, one in Finland and one in France, experienced significant delays and cost overruns. However, lessons learned from these experiences have improved the design and construction process. Subsequent EPR projects, such as the one built in the UK, are expected to be more efficient and cost-effective [9].

Overall, while the N4 and Konvoi designs were impressive for their time, the EPR represents a significant advancement in PWR technology, with higher power output, more advanced fuel assembly design, and improved safety features.

2.1 Plant layout

The plant layout is shown in Fig. 1. The EPR plant comprises a reactor building, a fuel building, four safeguard buildings, two diesel buildings, a nuclear auxiliary building, a waste building, and a turbine building [9].

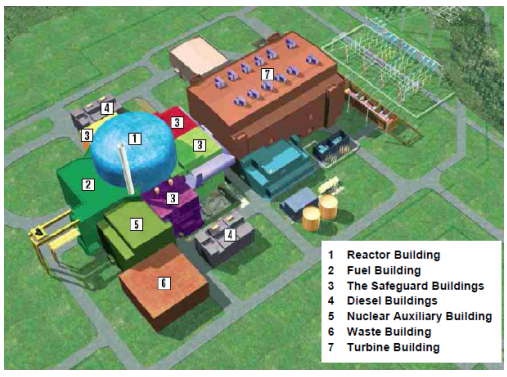

Figure 1: Typical plant layout [9].

The reactor building is surrounded by the four

safeguard buildings and the fuel building. The internal structures and components within the reactor building, fuel building, and two safeguard buildings (including the plant's main control room) are protected against aircraft hazard and external explosions. The other two safeguard buildings are not protected against aircraft hazard; however, they are geographically separated by the reactor building, which prevents both buildings from being simultaneously affected by such a hazard [9].

- Reactor building: The reactor building, located in the center of the Nuclear Island, houses the main components of the nuclear steam supply system (NSSS). Its primary function is to prevent the release of radioactive materials into the environment under all circumstances, including possible accident conditions. It consists of a cylindrical pre-stressed concrete inner containment with a metallic liner surrounded by an outer reinforced concrete shell. The primary system components are arranged within shielded areas within the reactor building [9].

- Fuel building: The fuel building, located on the same basemat that supports the reactor building and the safeguard buildings, and houses an interim fuel storage pool for fresh and spent fuel and associated fuel handling equipment [9].

- The safeguard buildings: The four safeguard buildings house key safeguard systems and their support systems. These safeguard systems are divided into four trains, each housed in a separate division in one of the four safeguard buildings. The main control room is located in one of the safeguard buildings [9].

- Diesel buildings: The two diesel buildings house the four emergency diesel generators and two station black-out diesel generators. Their support systems supply electricity to the safeguard systems in the event of a complete loss of electrical power. These two buildings' physical and geographical separation provides additional protection [9].

- Nuclear auxiliary building: The nuclear auxiliary building is located on a basemat separate from that supporting the reactor building. All air exhausts from the radiologically controlled areas are routed, collected, and controlled within the nuclear auxiliary building before being released through the stack [9].

- Waste building: The waste building is used for collecting, storing, treating, and disposing of liquid and solid radioactive waste and is adjacent to the nuclear auxiliary building [9].

- Turbine building: The turbine building contains the components of the steam-condensate feedwater cycle, including the turbine and generator set. The turbine building is independent of the nuclear island such that internal hazards in the turbine building remain confined. The building is located in a radial position concerning the reactor building to protect it from turbine missile impact [9].

The balance of plant (BOP) is an essential component of a nuclear power plant that supports the main reactor system. One critical aspect of the BOP is the main steam system (MSS), which transfers steam generated in the steam generators (SGs) to drive the electric generator. After exiting the SGs, the steam is dried and reheated in moisture separator/reheater units before entering three low-pressure turbines, which drive the electric generator. The steam exiting the turbines is condensed by water circulating through the condenser tubes, and the resulting water is cleaned and sent back to the SGs. The main feedwater system also contributes to supplying feedwater to the SGs. The system consists of a feedwater tank, feedwater pumps, high-pressure feedwater heaters, and feedwater isolation valves, which provide reactivity control in case of accidents [9].

The MSS and main feedwater system in a nuclear power plant require numerous safety measures to ensure safe operation. The main steam line has multiple safety and isolation valves to control steam flow and pressure in case of overpressure. Similarly, the main feedwater system has isolation valves with emergency backup power to control reactivity during a station

blackout. In case of an imbalance between turbine load and power or a reactor trip, turbine bypass valves allow excess steam to be dumped directly into the main condenser, ensuring the system can handle unexpected events. The following sections on safety systems discuss the aforementioned phenomena in greater detail [9].

2.2 Reactor core

The reactor core houses the fuel where fission reactions generate energy. The fuel assemblies are supported by internal structures that direct coolant flow and guide control rods, which regulate the reaction. The core is cooled and moderated by pressurized water at around 300°C with soluble boron as a neutron absorber. Gadolinium burnable absorber-bearing fuel rods adjust initial reactivity and power distribution. Instrumentation inside and outside the core monitors nuclear and thermal-hydraulic performance for control and protection functions. The core is designed for high thermal efficiency, flexible fuel cycle lengths, and load following [9].

- The reactor core contains 241 fuel assemblies that use uranium dioxide pellets stacked in cladding tubes with enrichment of up to 5% ^{235}U. MOX fuel can also be used. Some important parameters of EPR are depicted in Tab. 3 [9]. The EPR fuel design is highly reliable and has a low proportion of fuel rod failures. Even if fuel damage occurs, the mechanical integrity is preserved, and the fuel remains inside the cladding. The low power density of the core allows for flexible fuel cycle lengths between 1 and 2 years and efficient fuel use. For an 18-month fuel cycle, the amount of natural uranium required is limited to around 20 te/TWhe. Typical fuel assembly and rod schematics are shown below in Fig. 2 and Fig. 3, respectively.

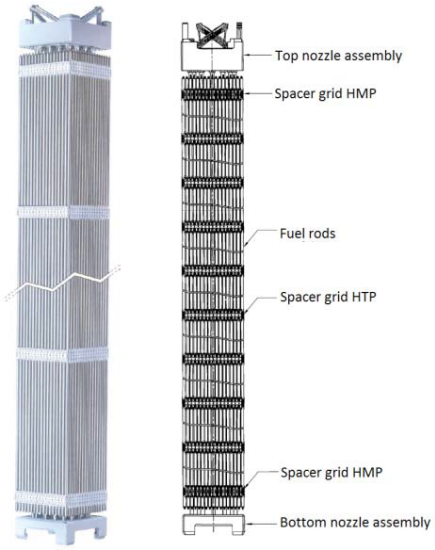

Figure 2: Fuel assembly [9].

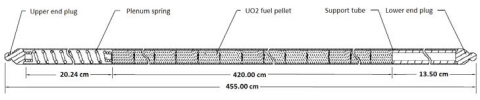

Figure 3: Fuel rod [9].

- To determine the nuclear power level in the core, primary heat balance and neutron flux measurements from the ex-core instrumentation are used. The ex-core instrumentation also detects criticality and power imbalances between core quadrants. The "Aeroball" system, which involves inserting vanadium alloy steel balls into the core and using activation measurements to determine local neutron fluxes, is used as reference instrumentation to periodically establish the power distribution in the core and construct a three-dimensional power map. Neutron detectors and thermocouples are used as fixed in-core instrumentation to continuously measure the neutron flux distribution and the margin-to-saturation in post-accident or degraded thermal-hydraulic conditions [9]. Fig. 4 is used below to show this graphically.

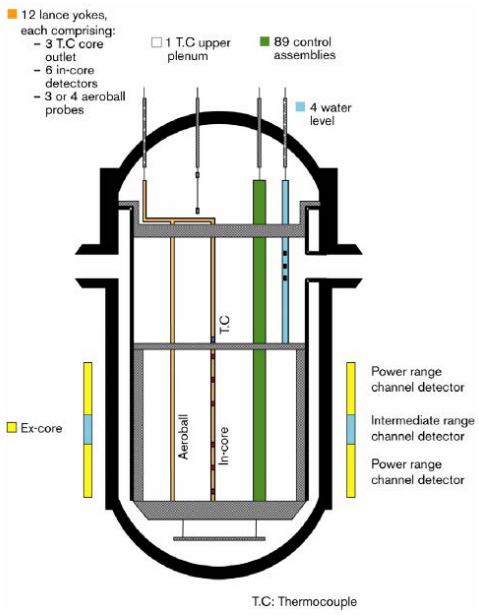

Figure 4: In-core and ex-core instrumentation of reactor core [9].

- The fuel handling system regularly replaces the reactor core's fuel assemblies with new ones. The spent fuel assemblies are then transported and stored in the spent fuel pool. The fresh and spent fuel assemblies are stored underwater racks, although a dry rack is only available for new fuel storage. The pool's capacity allows storing spent fuel generated over at least a 10-year operation period before export [9].

2.3 EPR nuclear systems

The EPR nuclear systems are mainly located in the reactor, fuel, and safeguard buildings. These buildings are robust and shielded where necessary to ensure all radioactive substances are always secure, and the systems include:

- reactor coolant system (RCS)
- fuel handling and storage system
- shut-down and reactivity control systems
- emergency core cooling systems (ECCS), containment cooling system (CCS), chemical and volume control system (CVCS), in-containment refueling water storage tank (IRWST). [9]

2.4 Reactor coolant system (RCS)

The core with fuel assemblies is located in the reactor pressure vessel (RPV) at the center of the reactor building. The reactor coolant flows through hot-leg pipes to the steam generators (SGs) and then back to the RPV through cold-leg pipes by the reactor coolant pumps (RCPs). The pressurizer (PZR) connects one hot leg through the surge line and two cold legs through the spray lines [9].

- The reactor pressure vessel (RPV) is the RCS's primary component. It is a cylindrical structure with a hemispherical bottom welded and a removable-flange-hemispherical upper head with a gasket. The RPV houses the reactor core, control rods, neutron shield, and supporting and flow-directing internals. The RPV is constructed of low-alloy steel and coated with stainless steel cladding for corrosion resistance. Cold legs transfer the coolant to the inlet nozzles at the vessel's bottom, flow through the annulus between the core barrel and inner vessel wall, then into the RPV outlet nozzles and towards the SGs. The RPV closure head has control rod drive mechanisms, level measurement, in-core instrumentation, dome temperature, and venting pipes. The RPV is fully supported to ensure its ability to withstand the forces generated during both design basis and severe accidents and seismic events [9]. The RPV internals is shown in Fig. 5, and some typical parameters are depicted in Tab. 1 in the context of UK EPR.

Table 1: Vessel design parameters for UK EPR [9].

General design	
Type	Four loops
Number of control rod mechanism adapters	89
Number of internal core instrumentation adapters	16
Number of flange studs	52
Calculation and operating conditions	
Design pressure	17.6 MPa abs.
Operating pressure	15.5 MPa abs.
Design temperature	351^oC
Temperature in the RCP [RCS] hot leg	328.1^oC
Temperature in the RCP [RCS] cold leg	295.5^oC
Test conditions	
Hydro-static test pressure	25.1MPa abs.
Hydro-static test temperature	$RT_{NOT} + 30^oC$
Sizes and weights	
Inner diameter of the cylindrical vessel	4870 mm
Outer diameter of the flange	5750 mm
Largest diameter (for transport)	7470 mm
Total height of the lower section (from flange to bottom of the dome)	10532.5 mm
Total height, head, control rod adapters, and venting tube included	13722.5 mm
Vessel body weight	410 t
Vessel height weight	116 t
Weight of studs, bolts and washers	32 t

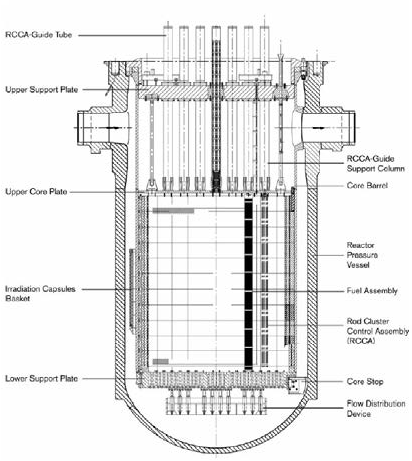

Figure 5: Reactor pressure vessel and its internals [9].

- The pressurizer is responsible for controlling the pressure of the RCS and acts as a coolant expansion vessel. It comprises a vertical cylindrical shell with hemispherical heads at both ends. The spray system inside includes main and auxiliary spray nozzles, with the main ones connected to cold legs and the auxiliary one connected to the CVCS. Electric heater rods are also included, and the upper head has multiple nozzles for safety valve connections, a pressurizer depressurization system line, and venting. It is connected to the RCS through a surge line and two spray lines connected to separate cold legs [9].

- The steam generators (SGs) are heat exchangers

with integral moisture-separating devices, and they have a vertical shell and a U-tube design that uses natural circulation. The reactor coolant flows through the inverted U-tubes and enters and exits through nozzles located in the hemispherical bottom channel head of the SG (as shown in Fig. 6). The heat from the reactor coolant is transferred to the secondary fluid through the tube walls of the tube bundle. The feedwater is directed to the cold side of the tube sheet by an annular skirt, which is injected by the feedwater distribution ring. This design improves heat exchange efficiency between the primary and secondary sides. Inconel 690 is the tube material because of its high corrosion resistance [9].

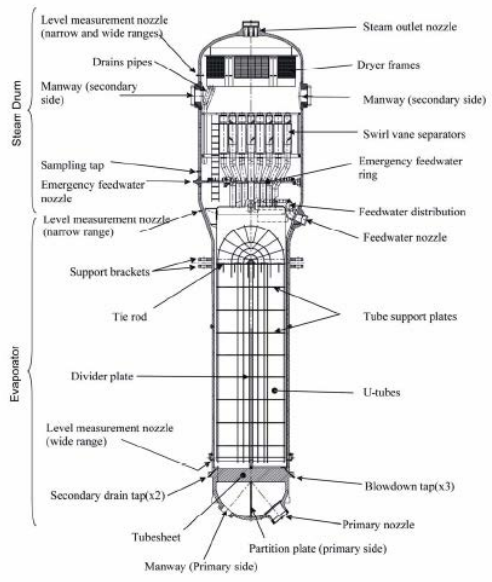

Figure 6: Steam generator [9].

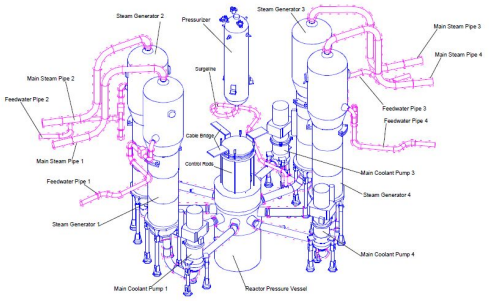

Figure 7: Primary circuit installation (3D) including pumping system [9].

- The reactor coolant pumps (RCPs) are single-stage vertical units driven by air-cooled, three-phase induction motors and equipped with shaft seals. The entire assembly comprises a motor, a hydraulic unit, and a seal assembly. The shaft seals have a standstill seal system (SSSS) to prevent leakage [9].

- Each of the four coolant loops in the reactor coolant system includes three components: a hot leg, a crossover leg, and a cold leg. The hot leg goes from the RPV to the SG, the crossover leg goes from the SG to the RCP, and the cold leg goes from the RCP to the RPV. The coolant system has been designed to use forged pipework and components and high mechanical performance materials to prevent major reactor coolant pipework rupture and to allow for early leak detection and in-service inspections. As a result, the rupture of major reactor coolant pipework is not included in the design basis [9].

3 Safety systems

The safety systems and functions have been designed with the following principles in mind: separation of operational and safety functions to simplify; four-fold redundancy in safeguard systems and their support systems to ensure high plant availability factor and ease of maintenance during plant operation; strict physical separation of buildings where the different

trains of safety systems are located; and the application of systematic functional diversity to ensure that there is always a diverse system available that can perform the desired function and bring the plant back to a safe condition even in the highly unlikely event of all redundant trains of a system becoming unavailable [9].

3.1 Chemical and volume control

To connect the high-pressure RCS and low-pressure systems in the nuclear auxiliary building and fuel building, the chemical and volume control system (CVCS) is utilized. The CVCS enables the continuous release and intake of RCS water and regulates the RCS water inventory at the required level while also permitting modification of the soluble boron concentration [9].

3.2 Safety injection / residual heat removal

This system (SIS/RHRS) serves a dual purpose in normal operating conditions and accidents. During normal operations in RHR mode, it facilitates heat transfer from the RCS to the component cooling water system (CCWS) and transfers heat during cold shutdowns and refueling. In the event of an accident, the SIS, along with the CCWS and the essential service water system (ESWS), maintains the RCS core outlet and hot leg temperatures below 180°C following a reactor shutdown. When operating in safety injection mode during a postulated loss of coolant accident, the SIS injects water into the reactor core to compensate for the effects of the event [9].

3.3 In-containment refueling water Storage tank (IRWST)

The in-containment refueling water Storage tank (IRWST) is a large tank filled with borated water that can be used to fill various compartments during refueling, collect water in case of accidents, and supply water to different pumps and systems like containment heat removal system (CHRS), SIS, and CVCS pumps under fault conditions. A hypothetical core melt accident can also flood the area where corium is spreading [9].

3.4 Emergency feedwater system (EFWS)

The emergency feedwater system (EFWS) provides water to the steam generators if all other feedwater supply systems are unavailable [9].

3.5 Component cooling water system (CCWS)

The CCWS transfers heat from various systems and equipment in the reactor to the ultimate heat sink through the ESWS. These systems include safety-related and operational auxiliary systems [9].

3.6 Ultimate cooling water system (UCWS)

The UCWS system has multiple functions, including cooling the dedicated cooling system for managing severe accidents and serving as a backup for cooling the fuel pool [9].

Additional systems in the EPR nuclear power plant include the nuclear sampling system for collecting samples of gases and liquids, the vent and drain system for collecting waste, the steam generator blowdown system to prevent buildup, and waste treatment systems for solid, liquid, and gaseous wastes. The fire protection system of the EPR is based on the defense in depth principle to protect the public, environment, and plant personnel from fire and its impact on reactor operations. The heating, ventilation, and air conditioning systems (HVAC) aim to contain radioactive substances and reduce radioactive releases while maintaining appropriate conditions for equipment and personnel [9]. Fig. 8 illustrates the primary systems.

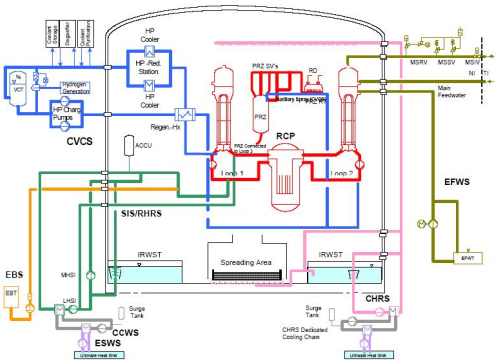

Figure 8: Main fluid systems [9].

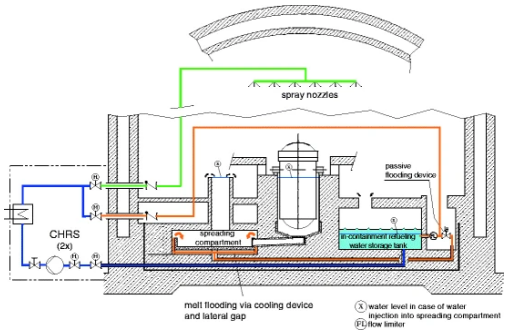

Figure 9: CHRS flow diagram [3].

3.7 Containment heat removal system (CHRS)

The containment heat removal system (CHRS) is an active system used in the EPR to remove decay heat from the containment in the long term. In the passive mode, steam generated from the decay heat is condensed back to the water, but active systems are needed for the long-term operation to avoid overpressure failure. The CHRS is equipped with active components and heat exchangers located outside the containment, and water is re-injected via spray rings in the upper containment. The CHRS can directly feed water into the core catcher, transporting the decay heat out of the containment by single-phase flow instead of evaporation and re-condensation, as depicted in Fig. 9. A unidirectional flow device, the Passive Outflow Reducer (flow limiter), is used to avoid a shortcut flow into the IRWST during active injection via the (open) passive flooding line [3].

3.8 Core catcher

In a meltdown, the core catcher plays a crucial role in preventing the molten core material, known as corium, from escaping into the surrounding environment. The core catcher is constructed from thermally resistant concrete ceramic that can withstand contact with corium without melting. In the EPR, the core catcher is positioned below the RPV, weighs 500 tonnes, and covers an area of 170 square meters. The core catcher is connected to the pressure vessel via a melt plug and a melt discharge channel, with the melt plug being automatically destroyed upon contact with the corium. The corium flows into a spreading compartment, cooled by expanding the available space. The spreading compartment can be flooded with water to enhance the cooling process. The core catcher comprises cast iron components containing cooling channels [3]. As depicted in Fig. 10, it is integral during passive and active modes.

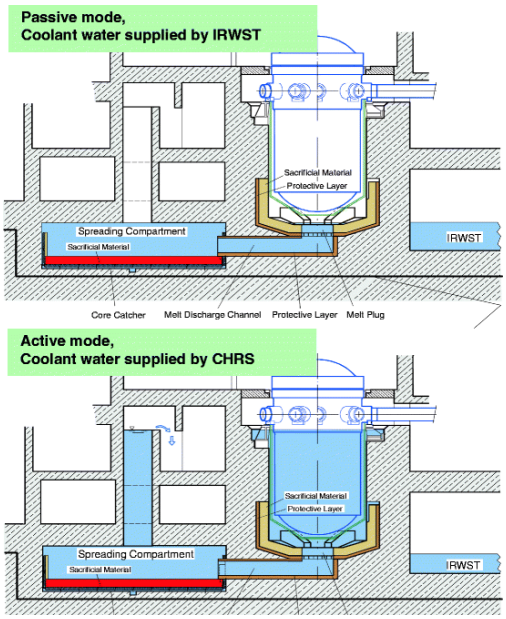

Figure 10: Passive and active mode of core catcher cooling [3].

3.9 Other safety systems

The extra boration system (EBS) is designed to maintain the required boron concentration in the reactor coolant system (RCS) for cold shutdown and has two independent trains. In the event of an accident and reactor trip unavailability, boric acid is automatically injected into the RCS. Some parts of the main steam system (MSS) and main feedwater system (MFWS) are also classified as safety systems [9].

4 Instrumentation and control system (I&C)

A nuclear power plant's instrumentation and control system comprises sensors, controllers, actuators, and monitors plant operators use. The EPR utilizes a computerized instrumentation and control system supplemented by a non-computerized safety system to ensure plant safety. The I&C systems adhere to redundancy, separation, and diversity principles. Operators use workstations and a plant overview panel in the main control room, with backup options available in case of failure or unavailability [9].

The EPR design includes appropriate instrumentation to cope with severe accidents. This instrumentation assists specific operator actions, surveys the effectiveness of the mitigation process, and monitors overall plant condition. All corresponding sensors, cables, and connectors are qualified for severe accident conditions. Depending on the specific licensing situation in the country the EPR is built in, other requirements may apply to the instrumentation, such as the requirement that the severe accident (SA) instrumentation and its power supply are independent of other instrumentation and power supplies or that the SA I&C has a separate, dedicated power supply backed up by batteries with sufficient capacity [3].

All severe accident-relevant information is displayed on a dedicated control panel. It includes signals that allow monitoring of various plant functions, such as depressurization of the primary circuit, core degradation and relocation, hydrogen control, core melt stabilization, containment heat removal system functions, and activity distribution within the plant and potential releases to the environment. The core melt stabilization system (CMSS) is passive. All related information is strictly informative to allow following the course of events and detecting of deviations from the mitigation path up to a potential failure of the CMSS function [3].

The CMSS-related part of the SA instrumentation consists of thermocouples located close to the outer side of the RPV lower head to detect whether RPV failure is imminent and/or has occurred in the chimney above the spreading area to detect melt arrival in the core catcher and in the core catcher's central water supply duct to detect core catcher melt-through and the threat of basemat penetration [3]. The main components of the CMSS system are shown in Fig. 11.

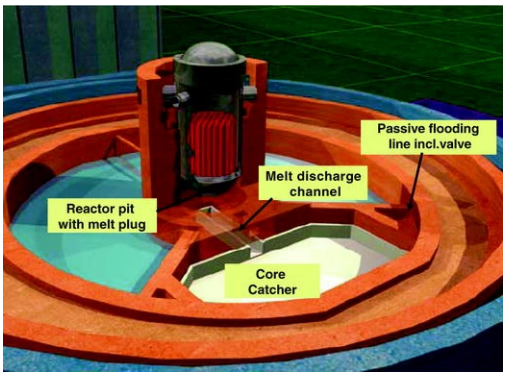

Figure 11: Main components for the core melt stabilization [3].

5 Electrical power system

To power, the EPR plant, a 50 Hz power supply is regulated by on-load tap changers via a site/utility-specific transmission grid. The electrical distribution system (EDS) is designed as a 4-train, 4-division system. The EDS's emergency power supply system (EPSS) ensures that safety systems are supplied with electrical power in case the preferred electrical sources are lost. Each train has an emergency diesel generator (EDG) set, and in case of total EDG loss, the station black-out (SBO) diesel generators supply the necessary power to emergency loads [9].

6 Nuclear safety

The process of nuclear fission generates a large number of radioactive materials that need to be protected for the safety of people and the environment. Nuclear safety involves the application of technical and organizational measures during the design, construction, and operation of a nuclear plant to reduce the likelihood and consequences of an accident [9].

Nuclear reactor safety depends on three essential functions:

- controlling the nuclear chain reaction and power generation,
- cooling the fuel, and
- containing radioactive materials [9].

Therefore, two fundamental principles of nuclear safety are:

- ensuring the existence of three protective barriers, and
- applying the concept of defense in depth [9].

6.1 Three protective barriers

To ensure nuclear safety, a series of strong, leak-tight physical barriers contain radioactive materials and prevent their release into the environment. These protective barriers include three layers: the first is the fuel, which is enclosed in metal cladding and traps most radioactive products. The second is the reactor coolant system, enclosed in a pressurized metal envelope that includes the reactor vessel containing the fuel rods. The third is the containment building, which houses the reactor coolant system and is designed as a double shell with a thick and leak-tight metallic liner covering the inner wall of the first shell [9]. Fig. 12 depicts the aforementioned protective barriers.

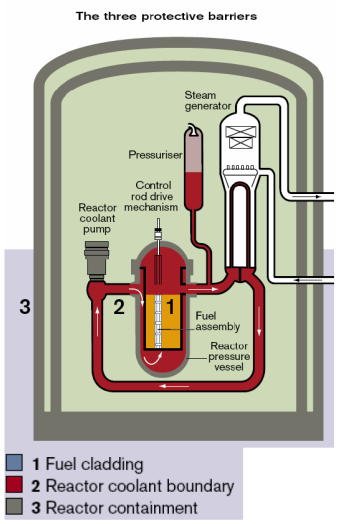

Figure 12: The three protective barriers [9].

6.2 Defense in depth

The principle of "defense in depth" involves protecting the protective barriers by providing multiple layers of defense against failures. The first layer involves implementing safe design, construction, and operation. The second layer involves monitoring for anomalies and detecting failures as soon as they occur. The third layer involves mitigating the consequences of failures and preventing core meltdowns using redundant systems. In a severe accident, a fourth layer of defense is provided to minimize the consequences [9].

The EPR safety approach for nuclear power plants is based on the deterministic application of the "defense in depth" concept, improved preventive measures, and innovations that reduce the probability of severe accidents. The design is supported by probabilistic analyses to identify accident sequences, evaluate their probability, and identify their potential causes and countermeasures. The safeguard systems are designed based on quadruple redundancy to minimize the risks from hazards such as earthquakes, flooding, fire, or aircraft crash. The policy of mitigating the consequences of a severe accident aims to "practically eliminate" situations that could lead to early containment failure or plant damage states (PDS) [9]. EDF/AREVA's targets and preliminary results for UK EPR are shown in Tab. 2.

6.3 Dose targets and legal limits (for UK EPR)

The legal limits for radiation doses to the public and workers in the UK are the same as the recommendations of the International Commission on Radiological Protection (ICRP) for a reactor during normal operation. The EPR reactor is expected to comfortably meet lower fundamental safety limits prescribed by the UK HSE for doses to worker groups. During normal operation, the EPR plant has a collective dose target of 350 man mSv/year, a small fraction of the dose target for earlier generation PWRs like the UK Sizewell B PWR. An assessment of the annual dose to the most exposed members of the public off-site due to the operation of an EPR reactor in the UK shows that the total annual dose is estimated to be 26μSv, well below the UK government limit of 300μSv. The EPR design complies with the HSE Basic Safety Objectives in all cases for doses to the public due to accidents [9].

7 Operation and maintenance (UK EPR)

During normal operation of a nuclear power plant, there may be scheduled changes in power load, unit shutdown/startup, or unplanned events like power source loss. The plant can also be shut down for maintenance, repair, fuel saving, or grid management. The shutdown mode depends on the nature of the intervention and duration, and during prolonged hot shutdowns, the boron concentration is adjusted for the shutdown margin. A cold shutdown is needed for refueling or maintenance. The main operating principles, from reactor shutdown to power operation for the next fuel cycle, are described chronologically. Operation with an extended cycle is also explained [9]. Moreover, the pressure-temperature graph for a typical UK EPR under general operating conditions is shown in Fig. 13.

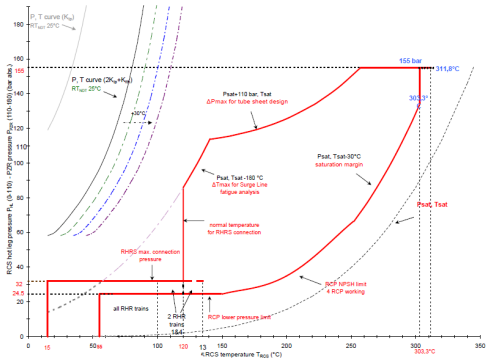

Figure 13: Pressure-Temperature graph for UK EPR under general operation condition [9].

Table 2: EDF/AREVA's targets and preliminary results for UK EPR [9].

Metric	Target /yr	Result /yr
Core Damage Frequency (CDF) internal events	10^{-6}	6.1×10^{-7}
CDF ext hazards	5×10^{-6}	5×10^{-7} (seismic) 7×10^{-8} (aircraft -FL3) 10^{-10} (industrial) 7×10^{-8} (extreme weather)
CDF internal hazards	10^{-6}	6.4×10^{-8} (fire) 2×10^{-8} (flood) Others to be added
PDS 3 (core damage with early containment failure)	10^{-7}	3.9×10^{-8}

7.1 Reactor shutdown

The reactor is initially in power operation mode at the end of a fuel cycle. The unit shutdown process starts by reducing the turbine load and tripping the turbine. The control rods are inserted manually to shut down the reactor, and the turbine bypass system controls the primary coolant temperature. The primary system is cooled to around 120°C, and the pressure is reduced to about 25 bar. The RIS-RRA [SIS-RHR] trains are started to continue cooling the primary system. The reactor refueling cavity slabs are removed below 120°C. The equipment hatch may be opened at 90°C, and the last primary pump is shut down when the radio-chemical criteria are met and the vessel head temperature is below 70°C. The primary system is maintained at 55°C, and boration is continued until the required boron concentration is achieved during the cold shutdown for fuel reloading. The primary pressure is reduced to 5 bar by auxiliary spray, and the pressurizer is maintained with a nitrogen gas bubble above the water [9].

7.2 Draining and opening the primary system

Before draining the primary system to $\frac{3}{4}$ loop level, one RIS [SIS] train in RRA [RHR] mode is stopped. The excess volume of primary coolant is transferred to TEP [CSTS] storage tanks for recycling. The RCP [RCS] is swept and vented before opening the primary system. The electrical connections of the rod control system mechanisms and core instrumentation are removed, and the mechanical seals are opened. After removing its thermal insulation, the vessel head is opened using a multistud tensioning machine (MSDG) [9].

7.3 Core unloading

During the removal of the vessel head, borated water from the IRWST is used to fill the compartments of the reactor refueling cavity. The core instrumentation and rod control system mechanisms are disconnected, and fuel unloading can begin after approximately 70 hours. Fuel unloading takes around 40 hours, and an engineered safeguard train may be unavailable during this time for maintenance. During this process, the PTR must be started to maintain the pool temperature below 50°C. After unloading, maintenance work is carried out, including inspection of steam generator tubes and fuel elements if needed [9].

7.4 Core reloading

The steam generator manways are closed, and the vessel refueling cavity is filled with borated water from the IRWST using the ISBP pumps. Then, the sluice gates are removed, and fuel is loaded into the vessel using the handling devices. The RIS in RRA mode maintains the primary temperature below 50°C during the 45-hour core loading and mapping operations. After loading, the transfer tube is closed, and

the upper internals, rod cluster control assemblies, aeroball lances, and core instrumentation are reinstalled [9].

7.5 Closing and filling the primary coolant system

The spent fuel pool compartments in the reactor building are emptied using the PTR's purification pumps, filters, and demineralizers [FPPS/FPCS], and the water is transferred to the IRWST. The reactor vessel is cleaned, closed with the MSDG, and reconnected to the primary system. The primary system is drained and filled using the RCV [CVCS] pumps and degassed by related systems. The conventional island operations are also completed, including filling the feedwater plant and steam generators, creating a vacuum in the condenser, and starting heating and chemical treatment [9].

7.6 Heating the primary coolant

The pressurizer is heated using heaters to raise primary pressure without exceeding 30 bar after shutting off the vacuum-creating device. The primary coolant is heated using the four pumps and fuel decay heat. The heating rate is limited to 50°C/hr. The secondary circuit is made available at the same time. The steam generators are filled, and the feedwater plant is heated and chemically treated. The excess coolant volume is drawn off through the RCV letdown line. Tests may be conducted during heat up, and at hot shutdown, the pressurizer level is set to its no-load set-point. The pressurizer heaters and steam generators control the pressure and temperature. The turbine generator unit is on its barring gear [9].

7.7 From hot shutdown to power operation

Before criticality, safety functions for power operation must be available. Tests such as rod drop time measurement are conducted during the hot shutdown. GCT [MSB] automatically controls the primary coolant temperature. Tests at zero power are done, and demineralized water is injected from the REA [RBWMS] using the RCV [CVCS] charging pumps to dilute the primary coolant. Power is increased by controlling the flux level. The startup and shutdown pump (AAD [SSS]) supplies the steam generators, followed by the feedwater pumps (APA [MFWPS]) using the normal feedwater flow control system (ARE [MFWS]). The turbine is commissioned and connected to the main grid, gradually increasing power. The normal steam generator control mode takes over flux level control. All RCP [RCS] controls are in automatic mode, gradually increasing power to 100% [9].

7.8 Power operation- load following

During normal operation, the primary coolant only needs to be diluted gradually to a boron concentration of 5-10 ppm at the end of the fuel cycle to compensate for long-term reactivity effects such as fuel burnup and samarium buildup. If necessary, the power plant may have to reduce power and resume full power production later. Steam generator control is automatic, and rod cluster control assemblies compensate for rapid reactivity changes through temperature control and power distribution. Boron concentration or rod cluster control assemblies are adjusted to compensate for slow variations in reactivity. The primary coolant is also chemically treated to meet the chemical and primary activity criteria, and fluid volumes may be recycled or directed toward waste treatment to avoid tritium buildup in the primary system [9].

7.9 Extended cycle operation

During power operation, primary boration compensates for available reactivity, with the boron content reduced as burnup increases until it reaches close to zero at the end of the cycle. To extend power operation beyond the natural end of the cycle, the decrease in reactivity due to fuel depletion may be compensated for by reducing the primary temperature. When control rods are mainly extracted and turbine inlet valves fully open, the power level is determined by core reactivity balance and turbine characteris-

tics. There is no built-in reactivity to maintain a constant average primary coolant temperature, and reactor power and steam pressure decrease steadily. Primary coolant mass is constant during power operation, so the drop in primary temperature requires a re-adjustment of main parameters. Extended cycle operation consumes the remaining built-in reactivity through repeated set-point adjustments. The pre-operational safety report will present studies of a cycle extended by up to 70 EFPD and early shutdown of 30 EFPD [9].

7.10 Reactivity-control systems

There are two methods used to control reactivity in nuclear reactors. The first method involves adding boron to the RCS to counteract slow reactivity changes. The second method involves using control-rod clusters, which contain a neutron-absorbing alloy and can be inserted or removed from the core to control reactivity. When the reactor temperature drops, reactivity in the core increases, and boron concentration is increased to compensate for the control rods' inability to control reactivity. Boric acid is injected into the RCS during plant operation or shutdown using the CVCS system [9].

7.11 Specific operations

Suppose an event occurs unrelated to an incident or accident, and the standard guidelines are inappropriate for handling the situation (such as during routine maintenance or power loss). In that case, the operators must follow specific event management guidelines [9].

7.12 Preventive maintenance

Maintenance is a set of technical, administrative, and management actions taken during the service life of the equipment to ensure that it performs its required function. Preventive maintenance aims to reduce the likelihood of equipment failure. The objectives of safety, availability, and cost must be achieved while adhering to regulations and protecting the environment, staff safety, and radiation protection. Requalification tests are carried out after maintenance operations to ensure equipment operates correctly. Design requirements are necessary to meet availability objectives and safety goals, and aspects related to radiation protection, operating costs, and availability must be considered during maintenance tasks. The design of the EPR takes into account several factors, such as engineered safeguard trains, PTR trains, and pressurizer conditions [9].

Designing a maintenance program during the design phase of an installation using the FMD approach can positively contribute to safety, unit availability, the environment, radiation protection, and human factors. The program should match maintenance activities to the importance and risk of the actual systems and equipment and comply with safety, availability, dosimetry, and cost objectives. The FMD approach aims to optimize preventive maintenance programs on equipment declared safety-critical while enhancing availability and meeting maintenance-related constraints. During the in-depth design study stage, adjustments can be made to equipment technology, systems, instrumentation, and condition monitoring. Developing maintenance programs requires ensuring compatibility and feasibility concerning the duration of work, accessibility of work zones, intervention dosimetry and decontamination, isolations, draining durations, and system startup. It is essential to differentiate between equipment for which maintenance may occur while the unit is in operation and equipment that must be carried out during the unit shutdown. Optimizing maintenance programs while meeting safety, availability, and environmental requirements is key [9].

8 Thermodynamic analysis

The axial distribution analysis is integral to calculating selected core parameters for a pressurized water reactor (PWR). This involves collecting data on key core parameters such as total core heat output, nominal system pressure, number of fuel assemblies, and more. With this data, several core-averaged thermal-hydraulic characteristics, such as axial pressure drop distribution, axial coolant enthalpy distribution, and

Table 3: UK EPR important parameters [9].

Parameters	Values
Total core heat output (95% of core heat output of original 4500 MW_{th})	4275 MW_{th}
Total heat output in fuel pellets (assumed 94.5% of the total core heat output)	4039.875 MW_{th}
Nominal system pressure	155 bar
Total core mass flow rate	22225 kg/s
Effective fuel cooling mass flow rate (= total mass flow rate minus bypass flow)	21002 kg/s
Core average mass flux	3560 kg/m^2s
Flow rate for one assembly	92.22 kg/s
Number of fuel assemblies	241
Number of fuel rods per assembly	265
Active fuel height	4.2 m
Lattice pitch	12.6 mm
Outside fuel rod diameter	9.5 mm
Clad thickness	0.57 mm
Fuel pellet diameter	8.19 mm
Number of spacers with a local loss coefficient of 0.8 each	10
Spacer uniformly distributed distance	0.382 m
Clad and channel wall roughness	0.001524 mm

axial coolant temperature distribution, must be calculated and presented as plots. Additionally, the flow characteristic of the core must be studied for core power levels ranging from 0% to 150% of the nominal power, with flow varying from 1% to 150% of the core nominal flow. Proper inlet orifices should be applied to stabilize flow through the core and avoid hydrodynamic instabilities.

8.1 Axial linear power distribution

Nuclear reactor rod bundles have a complex geometry, which requires advanced computational tools for a comprehensive thermal-hydraulic analysis. Different levels of approximations can be used, such as a simple one-dimensional analysis of a single subchannel or a fuel assembly, an analysis of the entire fuel assembly using a sub-channel analysis code, or a complex three-dimensional analysis using Computational Fluid Dynamics (CFD) codes. This report focuses on the simple approach, where a single sub-channel or a fuel assembly is treated as a one-dimensional channel with an equivalent hydraulic diameter.

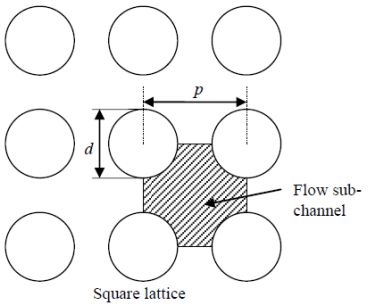

Figure 14: Typical coolant sub-channels in rod bundles [1].

The PWR's isolated subchannel model was utilized to obtain crucial parameters such as mass flux, hydraulic diameter, and heated perimeter for further computations. Fig. 14 illustrates the subchannel's geometry for a square lattice. Eq. (1) was initially employed to calculate the subchannel area based on the given subchannel geometry [1].

$$A = p^2 - \frac{\pi D_r^2}{4}, \tag{1}$$

where A is the subchannel flow area, D_r is the outer fuel rod diameter, and p is the lattice pitch.

On the other hand, the whole-assembly approach for thermal-hydraulic analysis approximates the entire fuel assembly as a one-dimensional channel, using global parameters such as hydraulic diameter, heated length, wetted perimeter, heated perimeter, and total flow area. The internal structure of the assembly is not considered in this approach. The heated perimeter is the total perimeter of all the rods in the fuel assembly that are in contact with the coolant and are generating heat. Suppose it is assumed that all rods are heated. In that case, the heated perimeter can be calculated by multiplying the number of rods in the assembly by the circumference of one rod, given by the formula:

$$P_H = N\pi d \tag{2}$$

and the corresponding heated diameter is as follows,

$$D_H \equiv \frac{4A}{P_H} = \frac{4w^2 - N\pi d^2}{N\pi d}. \tag{3}$$

Using the known coolant flow rate per fuel assembly, the proportion of the subchannel area to the total fuel assembly area was utilized to estimate the coolant flow rate per subchannel. Subsequently, the mass flux was determined using the equation below [1].

$$G = \frac{W}{A}, \tag{4}$$

where G is the mass flux and W is the coolant mass flow rate in the subchannel.

Therefore, the heated perimeter [1] was found as,

$$P_H = \pi D_r, \tag{5}$$

where P_H is the heated perimeter.

Then from that, the hydraulic diameter was determined using the formula for the square lattice [1]

$$D_h = D_r \left[\frac{4}{\pi} \left(\frac{p}{D_r} \right)^2 - 1 \right], \tag{6}$$

where D_h is the hydraulic diameter.

Various shapes of axial power distribution may exist in nuclear reactor cores. In cylindrical homogeneous reactors, a cosine-shaped power distribution, from [1], is obtained by applying the diffusion approximation for neutron distribution calculation.

$$q''(r,z) = q_0'' J_0 \left(\frac{2.405r}{\tilde{R}} \right) \cos\left(\frac{\pi z}{\tilde{H}} \right), \tag{7}$$

where q_0'' is the heat flux at the core center $r = z = 0$, J_0 is the Bessel function of the first kind and zero order, and $\tilde{R}$, $\tilde{H}$ are the extrapolated radius and the extrapolated height of the core, respectively.

The peaking factor is the ratio of a reactor core's maximum to average power densities. The peaking factor [1] can be calculated for the whole core volume:

$$f_V = \frac{q_0'''}{\bar{q}'''} = \frac{q'''(0,0)}{\frac{1}{\bar{V}} \int_V q''' dV}$$

where q_0''' and q''' power density at the core center $r = z = 0$ and overall power density respectively.

In a cylindrical core, we have in addition radial and axial peaking factors:

$$f_R(z_P) = \frac{q'''(0,z_P)}{\frac{1}{\pi R^2} \int_0^R q'''(r,z_P) 2\pi r dr} \quad f_A(r_P) = \frac{q'''(r_P,0)}{\frac{1}{H} \int_{-H/2}^{H/2} q'''(r_P,z) dz}$$

Here z_P and r_P are fixed values of the axial and radial coordinates at which peaking factors are defined.

For example, for a fuel rod located at $r = r_P$ distance from the center line, the axial peaking factor is found as

$$f_A(r_P) = \frac{q_0''' J_0\left(\frac{2.405 r_P}{\tilde{R}}\right) \cos(0)}{\frac{1}{H} \int_{-H/2}^{H/2} q_0''' J_0\left(\frac{2.405 r_P}{\tilde{R}}\right) \cos\left(\frac{\pi z}{\tilde{H}}\right) dz}$$
$$= \frac{1}{\frac{1}{H} \int_{-H/2}^{H/2} \cos\left(\frac{\pi z}{\tilde{H}}\right) dz} = \frac{\pi H}{2\tilde{H} \sin\left(\frac{\pi}{2} \cdot \frac{H}{\tilde{H}}\right)}.$$

Similarly, for a core cross-section located at $z = z_P$,

the radial peaking factor is found as

$$f_R(z_P) = \frac{q'''_0 J_0(0)\cos\left(\frac{\pi z_P}{\tilde{H}}\right)}{\frac{1}{\pi R^2}\int_0^R q''_0 J_0\left(\frac{2.405r}{\tilde{R}}\right)2\pi r\cos\left(\frac{\pi z_P}{\tilde{H}}\right)dr}$$
$$= \frac{1}{\frac{1}{\pi R^2}\int_0^R J_0\left(\frac{2.405r}{\tilde{R}}\right)2\pi r dr} = \frac{2.405\cdot R}{2\tilde{R}\cdot J_1\left(\frac{2.405R}{\tilde{R}}\right)}.$$

As it can be seen that both the radial and the axial peaking factor do not depend on z_P and r_P. Here, z_P and r_P are fixed values of the axial and radial coordinates at which peaking factors are defined

The spatial core power distribution is assumed as (7), and for the reflected core, it can be assumed that

$$\frac{R}{\tilde{R}} \cong \frac{H}{\tilde{H}} \cong \frac{5}{6}.$$

The average linear power per fuel rod was determined from the total core power and the total number of fuel rods, as shown below.

$$q'_{avg} = \frac{Q_{total\_core}}{N_{rod}\times L_{rod}} \tag{8}$$

where q'_{avg} is the average power per rod, Q_{total_core} is the total core heat output, N_{rod} is the total number of fuel rods in the core, and L_{rod} is the active fuel rod length.

We can get the linear power as a function of axial position, as shown below

$$q'(z) = q'_0\cos\left(\frac{\pi z}{\tilde{H}}\right) \tag{9}$$

where $q'(z)$ is the linear power of the fuel rod at axial position z (ranging from $-H/2$ to $H/2$ given that H is the active fuel length from Tab. 3) and q'_0 is the maximum linear power per rod and given as

$$q'_0 = q'_{avg}\times f_A. \tag{10}$$

Similarly for hot channel, the $q'(z)$ changes as the q'_0 now then becomes

$$q'_{0,hot} = q'_{avg}\times f_A \times f_R. \tag{11}$$

8.2 Axial coolant enthalpy distribution

Suppose a channel is heated with an arbitrary heat flux distribution $q''(z)$ along the axial direction. The channel geometry also varies axially, as illustrated in Fig. 15. The mass flow rate of the coolant flowing through the channel is constant and denoted by W.

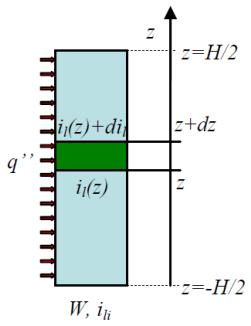

Figure 15: A heated channel [1].

The amount of energy in a heated channel between two points, z and $z+dz$, can be expressed using an energy balance equation:

$$W\cdot i_l(z) + q''(z)\cdot P_H(z)\cdot dz = W\cdot\left[i_l(z)+di_l\right],$$

where W is the constant mass flow rate of the coolant, $q''(z)$ is the heat flux, $P_H(z)$ is the heated perimeter of the channel, $i_l(z)$ is the coolant enthalpy at location z, and di_l is the change in enthalpy over the length dz.

Solving for di_l results in the following differential equation for the coolant enthalpy:

$$\frac{di_l(z)}{dz} = \frac{q''(z)\cdot P_H(z)}{W}. \tag{12}$$

Integrating this equation from the channel inlet ($z=-H/2$) to a particular location z yields the coolant enthalpy at that location:

$$i_l(z) = i_{li} + \frac{1}{W}\int_{-H/2}^{z} q''(z)\cdot P_H(z)dz, \tag{13}$$

where i_{li} is the coolant enthalpy at the inlet to the channel.

The integral part is implemented in the numerical analysis by discretization as follows:

$$i_{l,j} = i_{l,j-1} + \frac{q'_{j-1} \times z_{cell}}{W} \tag{14}$$

where $i_{l,j-1}$ is the coolant enthalpy of the previous cell to j-cell whose enthalpy is $i_{l,j}$, and z_{cell} is the cell span (in the case of axial considerations, we refer to it as cell height).

8.3 Axial pressure drop

The pressure drop along a fuel assembly can be caused by various mechanisms, including frictional losses from the fuel rod bundle, local losses from spacer grids, local losses at the core inlet and exit, and elevation pressure drop. The total pressure drop in a channel with a constant cross-section area can be determined using Eq. (15), which takes into account Fanning friction coefficient C_f, length of the channel L, mass flux G, channel hydraulic diameter D_h, and coolant density ρ. For single phase flow (which is valid to assume at nominal conditions for a PWR like the EPR), the equation [1] can be written as

$$-\Delta p_{\text{tot}} = -\Delta p_{\text{fric}} - \Delta p_{\text{loc}} - \Delta p_{\text{elev}} = \left(\frac{4C_{f,lo}L}{D_h} + \sum_i \xi_i\right)\frac{G^2}{2\rho} + L\rho g \sin\varphi \tag{15}$$

Fanning friction coefficient C_f, however, can be influenced by different flow patterns as it is shown to be dependent on Reynolds number, Re:

- for laminar flow ($\text{Re} < 2300$):

$$C_f = \frac{16}{\text{Re}}$$

- for turbulent flow (Blasius's formula, $10^4 < \text{Re} < 10^5$):

$$C_f = \frac{0.0791}{\text{Re}^{0.25}}$$

- for turbulent flow in commercial rough tubes (Colebrook's formula can be replaced with Haaland's formula):

$$\frac{1}{\sqrt{C_f}} = -3.6\log_{10}[(\frac{\frac{k}{D_r}}{3.7})^{1.11} + \frac{6.9}{\text{Re}}] \tag{16}$$

where k is the wall roughness and D_r is the rod diameter.

The pressure drop caused by spacer grids, coolant inlet, exit, and changes in bundle cross-section also contributes to additional pressure losses. These losses are called local pressure losses and can be calculated using the following general formula:

$$-\Delta p_{\text{loc}} = \xi_{loc}\frac{G^2}{2\rho} \tag{17}$$

where ξ_{loc} is the local pressure loss coefficient.

The loss coefficient for grid spacers, which represents the pressure loss associated with spacer geometry, is typically determined through experimental means. The value for the loss coefficient for a typical spacer is given by:

$$\xi_{space} = a + b\text{Re}^{-c} \tag{18}$$

where a, b, and c are constants determined experimentally. Since we cannot access these constants, we assumed the local loss coefficient value by converging the value of it as we know inlet orifices pressure loss in PWRs is 25% at nominal operating conditions (therefore, for each spacer, an assumption validated by the project description [4] was made). In hindsight, this might add some errors to the final calculations.

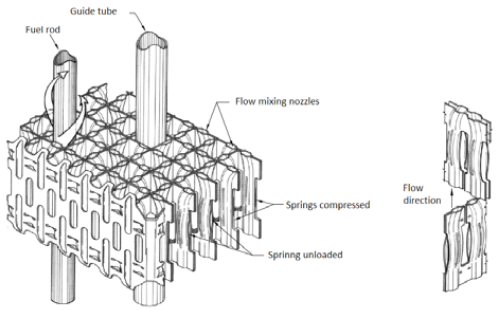

Figure 16: Part of spacer grids [6].

Different phases, namely one-phase and two-phase drop calculations techniques [1], are shown in the Tab. 4 where $C_{f,lo}$ and $C_{f,2\Phi}$ are the Fanning friction factors [1] for liquid only phase, i.e., one-phase and two-phase respectively. Moreover, the density

Table 4: Pressure drop for different phases.

Pressure drop	Single phase $x < 0$	Two phase $x \geq 0$
$-\Delta P_{fric}$	$\frac{4C_{f,lo}L}{D_h}\frac{G^2}{2\rho_f}$	$\frac{4C_{f,2\Phi}L}{D_h}\frac{G^2}{2\rho_m}$
$-\Delta P_{loc}$	$\sum_i \xi_i \frac{G^2}{2\rho_f}$	$\sum_i \xi_i \frac{G^2}{2\rho_m}$
$-\Delta P_{elev}$	$L\rho_f g \sin\varphi$	$L\rho_m g \sin\varphi$
$-\Delta P_{acc}$	0	$\frac{G^2}{2\rho_m}$

of mixture ρ_m and equilibrium quality x are further explained in Eq. (27) and Eq. (26) in section 8.2.

8.4 Axial coolant temperature distribution

Assuming that the temperature and pressure changes are small, the enthalpy of a non-boiling, single-phase coolant can be expressed as a linear function of the temperature. If there is a uniform axial distribution of heat sources and a constantly heated perimeter, then Eq. (13) can be simplified as follows:

$$T_{lb}(z) = T_{lbi} + \frac{q'' P_H (z + H/2)}{c_p W}, \tag{19}$$

where $T_{lb}(z)$ is the temperature of the coolant at location z, T_{lbi} is the coolant temperature at the inlet to the channel, c_p is the specific heat of the coolant, and H is the heated length of the channel.

The coolant's bulk temperature at a particular location is called $T_{lb}(z)$. It is defined as the temperature that can be determined from the energy balance of a section of the channel. This method works for any distribution of temperature, velocity, and fluid properties across the channel cross-section.

$$T_{lb} = \frac{\int_A \rho_l c_{pl} v_l T_l dA}{\int_A \rho_l c_{pl} v_l dA} \tag{20}$$

The Eq. (19) is limited to coolant that doesn't undergo a phase change, while Eq. (13) can be used for single-phase and two-phase flows. The local velocity in a channel cross-section is denoted by v_l whereas ρ_l and c_{pl} are its density and specific heat capacity at that location.

The temperature of the coolant changes linearly with the distance from the inlet to the channel. If we assume that the entire length of the channel is H, then we can calculate the exit temperature using the following equation:

$$T_{lbex} = T_{lbi} + \frac{q'' P_H H}{c_p W}$$

However, we know from Eq. (7) that in cylindrical homogeneous reactors, a cosine-shaped power distribution is obtained by applying the diffusion approximation for neutron distribution calculation. Eq. (7) and the coordinate system in Fig. 17 express the power distribution.

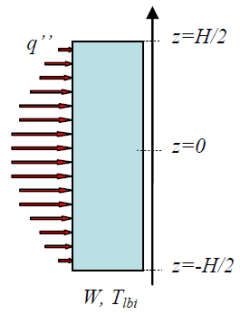

Figure 17: Heated channel with cosine power shape [1].

Eq. (12) then becomes,

$$\frac{di_l(z)}{dz} = \frac{q_0'' \cdot P_H(z)}{W} \cos\left(\frac{\pi z}{\widetilde{H}}\right), \tag{21}$$

and

$$\frac{dT_{lb}(z)}{dz} = \frac{q_0'' \cdot P_H(z)}{W \cdot c_p} \cos\left(\frac{\pi z}{\widetilde{H}}\right). \tag{22}$$

After integration, the coolant enthalpy and temperature distributions are as follows

$$i_l(z) = \frac{q_0'' \cdot P_H}{W} \cdot \frac{\widetilde{H}}{\pi} \left[\sin\left(\frac{\pi z}{\widetilde{H}}\right) + \sin\left(\frac{\pi H}{2\widetilde{H}}\right)\right] + i_{li}, \tag{23}$$

and

$$T_{lb}(z) = \frac{q_0'' \cdot P_H}{W \cdot c_p} \cdot \frac{\widetilde{H}}{\pi} \left[\sin\left(\frac{\pi z}{\widetilde{H}}\right) + \sin\left(\frac{\pi H}{2\widetilde{H}}\right)\right] + T_{lbi}. \tag{24}$$

The channel exit temperature and enthalpy can be found substituting $z = H/2$ into (24) and (23) as follows,

$$i_{\text{lex}} = i_l(H/2) = \frac{2q_0'' \cdot P_H \cdot \widetilde{H}}{\pi \cdot W} \sin\left(\frac{\pi H}{2\widetilde{H}}\right) + i_{li},$$

and

$$T_{lbex} = T_{lb}(H/2) = \frac{2q_0'' \cdot P_H \cdot \widetilde{H}}{\pi \cdot W \cdot c_p} \sin\left(\frac{\pi H}{2\widetilde{H}}\right) + T_{lbi}.$$

However, to simplify the integration process for the numerical method to obtain the temperature distribution just like it was done in Eq. (14) for enthalpy distribution, we can get an expression for temperature distribution calculations as shown below

$$T_{l,j} = T_{l,j-1} + \frac{q'_{j-1} \times z_{cell}}{c_p \times W} \tag{25}$$

where $T_{l,j-1}$ is the coolant temperature of the previous cell to j-cell whose temperature is $T_{l,j}$, and z_{cell} is the cell span (in the case of axial considerations, we refer to it as cell height). Moreover, c_p is the specific heat capacity of the coolant at that location which is dependent on that particular location's pressure and enthalpy, as found from calculations techniques enlisted in sections 8.2 and 8.3.

8.5 Flow characteristics

In thermal hydraulics, the behavior of a reactor core is described by the connection between core pressure drop and mass flux. The flow resistance through the core increases as the mass flux increases, which can be affected by factors such as fuel burnup, core geometry, and coolant properties. It is crucial to understand these flow characteristics for safe and efficient nuclear reactor operation. Deviations from expected flow behavior can impact core performance and potentially lead to safety concerns. The relationship between the axial pressure drops as a function of coolant mass flux was studied at various power levels, resulting in two-phase flow and the quality calculation (shown in Eq. (26)) in these regions [1].

$$x(z) = \frac{i(z) - i_f}{i_{fg}} \tag{26}$$

where $x(z)$ is the quality according to axial position, i_f is the enthalpy of the liquid at saturation and i_{fg} is the enthalpy of evaporation, i.e., $i_{fg} = i_g - i_f$.

When boiling was introduced, the method of calculating pressure drop was changed. Instead of the previous method, the Homogeneous Equilibrium Model (HEM) was utilized to calculate the density and dynamic viscosity of the liquid-vapor mixture [1]. The equations used for these calculations are given in Eq. (27) and Eq. (28).

$$\rho_m = \frac{\rho_f}{x\left(\frac{\rho_f}{\rho_g} - 1\right) + 1} \tag{27}$$

$$\frac{1}{\mu_m} = \frac{x}{\mu_g} + \frac{1-x}{\mu_f} \tag{28}$$

where the subscript m represents the mixture properties, g represents the properties of the vapor at saturation, and f represents the properties of the liquid at saturation.

The method for calculating pressure drop was the same as explained in Section 8.1, but with some changes for the two-phase flow regions (where $x > 0$). In these regions, μ_m was used for the Reynolds number calculation, while ρ_m was used in the pressure drop equation. Also, the acceleration pressure drop, which arises from the change in density during evaporation, had to be included. This was represented by Eq. (29).

$$-\Delta P_{acc} = \frac{G^2}{2\rho_m} \tag{29}$$

8.6 Critical heat flux (CHF)

The safety of pressurized water reactors (PWRs) relies on preventing a departure from nucleate boiling (DNB), which reduces heat transfer and can cause a rise in fuel temperature. Operators must maintain a safe margin to DNB by controlling plant parameters like reactor coolant pressure, flow rate, power, and inlet temperature. Limitations on global and local power distribution are important for safety, especially in limiting the local heat flux. This can cause heat transfer deterioration at the critical heat flux (CHF)

point. This is known as the boiling crisis, which occurs when nucleate boiling transitions to film boiling due to forming a vapor layer on the surface.

In sub-channel CHF correlation, Reddy and Fighetti developed a generalized sub-channel CHF correlation for both PWR and BWR fuel assemblies (both DNB and dry-out) [1]:

$$q''_{cr}(\mathbf{r}) = B\frac{A - x_{in}}{C + \frac{x(\mathbf{r}) - x_{in}}{q''_R(\mathbf{r})}}$$

$$A = a_1 p_R^{a_2} G_R^{(a_3 + a_4 p_R)} \quad G_R = G/1356.23$$
$$B = 3.1544 \times 10^6 \quad p_R = p/p_{cr}$$
$$C = c_1 p_R^{c_2} G_R^{(c_3 + c_4 p_R)} \quad q''_R(\mathbf{r}) = q''(\mathbf{r})/3.1544e6$$

where q_{cr} - critical heat flux, W/m^2, x_{in} - inlet equilibrium quality, G - mass flux, kg/m^{2}s, p-pressure, Pa, p_{cr} - critical pressure, Pa, r - location $a_1 = 0.5328, a_2 = 0.1212, a_3 = -0.3040$, $a_4 = 0.3285, c_1 = 1.6151, c_2 = 1.4066, c_3 = 0.4843, c_4 = -2.0749$.

We used the above correlation as the UK EPR parameters (from Tab. 3) fall in these applicability ranges of the aforementioned correlation except for mass flux, G value. Since none of the other correlations match many other criteria, we chose the closest and most reliable one.

$0.762 < L < 4.267$ m, $13.8 < p < 169.9$ bar,

$8.9 < D_h < 13.9$ mm, $6.3 < D_H < 13.9$ mm,

$-0.25 < x < 0.75, -1.10 < x_{in} \leq 0.0$,

$147 < G < 3023$ kg/m^{2}s

To determine if there is a departure from nucleate boiling in the hot channel, the ratio of CHF $q''_{cr}(z)$ and actual heat flux $q''(z)$ was found. This ratio,

$$\text{DNBR}(z) = \frac{q''_{cr}(z)}{q''(z)}$$

is called the departure from nucleate boiling ratio (DNBR) and departure from nucleate boiling occurs when it is equal to one. The minimum point of the DNBR is the minimum DNBR (MDNBR). It is the location where the fuel assembly is closest to departure from nucleate boiling and needs to be found to predict thermal margins.

8.7 Fuel assembly nodalization

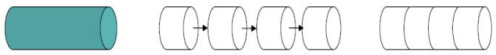

(a) Pipe discretization represented by control volumes.

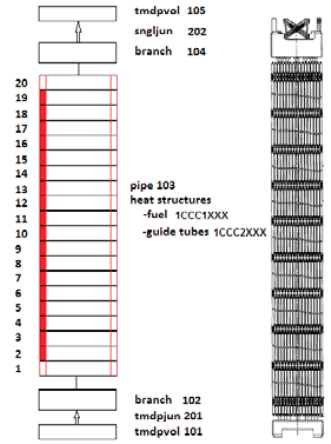

(b) Nodalization and the end view of a fuel assembly.

Figure 18: Fuel assembly nodalization [6].

The fuel assembly nodalization involves dividing the geometry into control volumes and solving equations for each fluid phase's mass, momentum, and energy balances. The algorithm (shown in Fig. 18) includes two main parts: energy balance and pressure drop calculation. In the energy balance part, the algorithm calculates the energy balance of each control volume by using the previous control volume's value, the cell flow rate, and the width of the control volume [6, 7].

In the pressure drop calculation part, the algorithm iteratively calculates the pressure drop across each control volume until it converges. The pressure drop is calculated based on the void fraction model, pressure drops across the cell, and the pressure of the previous control volume. The algorithm also calculates the temperature and flow characteristics of the core and the inlet orifice pressure loss coefficient [6, 7].

9 Core-averaged distributions

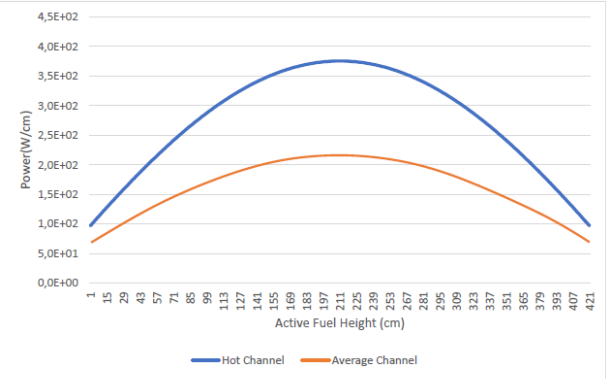

Axial peaking factor (-) 1.35	Radial peaking factor (-) 1.73
Hot channel 354,8 W/cm	Average Channel 204,1W/cm

Figure 19: Axial linear power distribution.

The power density distribution of the hot channel follows the same shape as the average configuration, and the position of maximum power is at the center of the rod. The ratio between the maximum linear power obtained for each configuration equals the ratio between the peaking factor applied in each case, as depicted in Fig. 19.

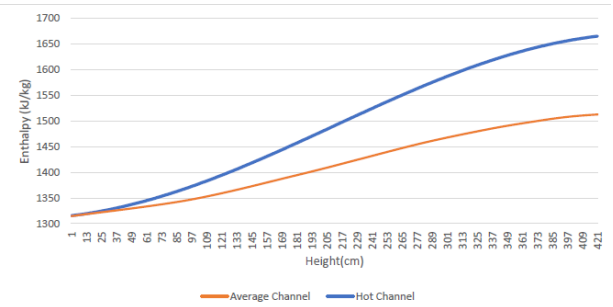

Figure 20: Axial enthalpy distribution.

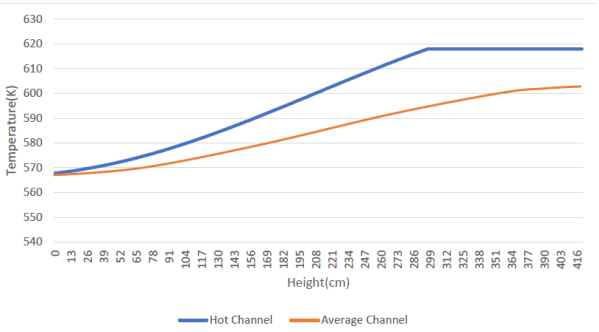

Figure 21: Axial temperature distribution.

The temperature distribution plotted using the hot channel follows the same shape as the temperature distribution from the average channel with higher temperature values until $z = 296$ cm as shown in Fig. 21. The coolant reaches its saturation temperature of 618 K (saturation temperature for 15.5 MPa). At this point, steam begins to form in the reactor, but the temperature does not continue to increase because the enthalpy is transformed into latent heat instead of sensible heat. The maximum coolant enthalpy value in the hot channel configuration has increased to 1665.39 kJ/kg. On average, the coolant enthalpy axial distribution is similar in shape to the hot channel distribution as depicted in Fig. 20. However, hot channel configurations with hot channel values are elevated due to the power increment as we considered the radial peaking factor.

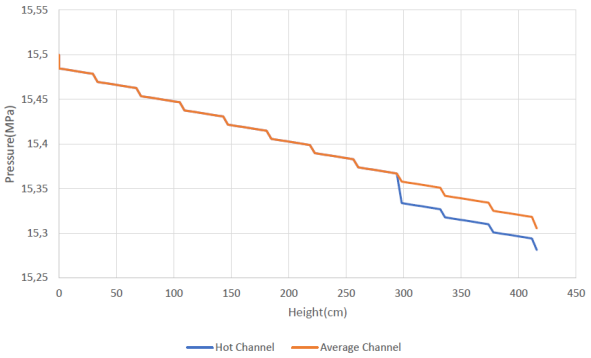

Figure 22: Axial pressure drop distribution.

In the single-phase flow region where the coolant is fully in the liquid state ($z < 298$ cm), the pressure drop follows the same evolution in the hot channel configuration as in the average channel configuration. However, when two-phase flow begins, the pressure drops increase, especially in the acceleration pressure drop. Although EPR is not designed to boil, in this calculation, it is observed that the hot channel reaches two-phase towards the top tail of the channel. The pressure losses in the axial profile along the active fuel height mentioned in Tab. 3 are plotted for the average channel and hot channel depicted in Fig. 23a and Fig. 23b.

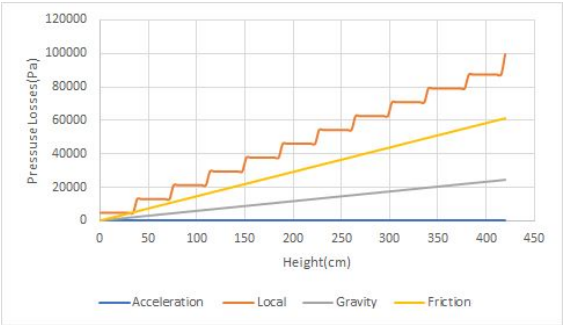

(a) Average channel.

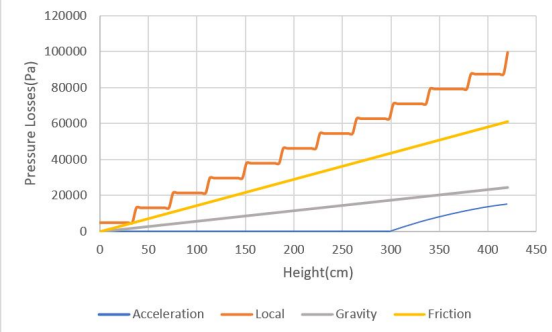

(b) Hot channel.

Figure 23: Axial distribution of pressure losses.

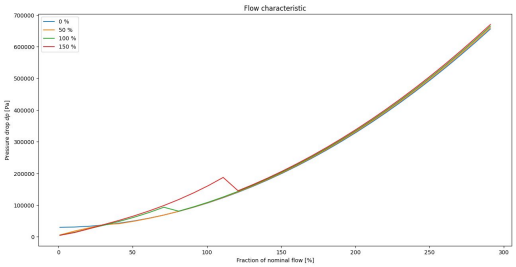

Figure 24: Flow characteristic of the core.

The flow characteristic of the core is a relationship $\Delta p_{core} = f(G_{core})$ where core pressure drop versus mass flux, for core power equal to 0%, 50%, 100% and 150% of the nominal power, with flow varying from 1% to 300% of the core nominal flow are plotted in Fig. 24. Single-phase steam was observed at very low flow rates for 150%, 100%, and 50% power, and 2-phase flow was observed at medium flow rates. An upward bump in the curve indicated the transition from single-phase steam to 2-phase flow. Single-phase water was observed at high flow rates, and a downward bump marked the transition from 2-phase flow to single-phase water. At 0% power, there was only continuous single-phase water due to the absence of heat energy. Interestingly, the total pressure was higher for 0% power at very low flow rates because of the presence of single-phase water instead of single-phase steam, leading to a higher gravity and friction pressure drops.

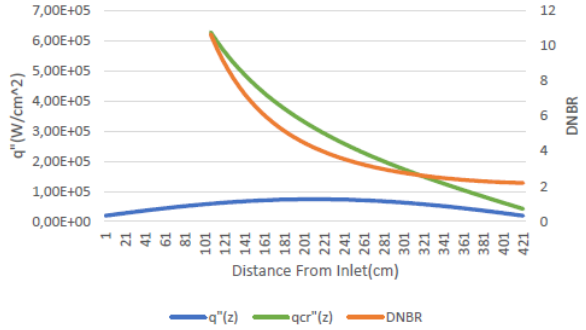

Figure 25: Axial critical flux and DNBR distribution.

A DNBR value of 1.0 indicates that the onset of nucleate boiling has just occurred, and any value below 1.0 indicates that boiling is occurring on the fuel rod surface. Therefore, a higher DNBR value indicates a greater margin of safety against boiling.

In the literature on general EPR design, the minimum DNBR (MDNBR) under nominal operating conditions is nearly 2.6 [9], which means there is a significant margin of safety against boiling on the fuel rod surface. However, in this project, with only 95% of core heat output from its actual value of 4500 MW_{th}, resulted in the MDNBR of 2.2 at a location 416 cm from the reactor core.

This indicates that even at this reduced power level, there is still a sufficient margin of safety against boiling on the fuel rod surface, as the MDNBR is still above the recommended value of 1.0. However, it is important to continuously monitor the DNBR during operation to ensure it remains above the recommended minimum and to take corrective action to prevent boiling on the fuel rod surface.

If there is steam in a PWR, it could cause damage to the fuel. Tab. 5 shows the exploration for a power setup where the EPR will never exceed its saturation temperature.

Table 5: Power for avoiding boiling in our configuration.

Power (MW_{th})	Location of T_{sat}(cm)
4500	283
4000	231
3600	357
3250	No boiling

10 Maximum cladding and fuel pellet temperature

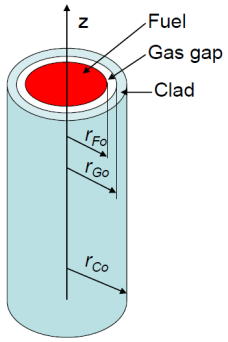

Figure 26: Typical cylindrical fuel element construction [1].

In the cylindrical coordinate system, for a fuel rod, as shown in Fig. 26, the conduction equation, from [1], can be written as

$$\nabla \cdot \lambda \nabla T = -q'''(r) \tag{30}$$

where q''' is the density of heat sources.

Then, Eq. (30) can be written in the form

$$\frac{1}{r}\frac{\partial}{\partial r}(r\lambda\frac{\partial T(r,z)}{\partial r}) + \frac{\partial}{\partial z}[\lambda\frac{\partial T(r,z)}{\partial z}] = -q'''(r) \tag{31}$$

The conduction equation can be further simplified:

- Heat conduction in the z direction can be neglected since temperature gradient $\frac{dT}{dz}$ is much lower than $\frac{dT}{dr}$.
- In fuel region, $q''' = q'''(z)$.
- In gas gap and clad regions, $q''' = 0$.

The conduction equation can be thus written for each region separately as:

- Fuel

$$\frac{1}{r}\frac{d}{dr}\left(r\lambda_F\frac{dT_F(r)}{dr}\right) = -q'''(z) \tag{32}$$

- Gap

$$\frac{1}{r}\frac{d}{dr}\left(r\lambda_G\frac{dT_G(r)}{dr}\right)=0$$

- Clad

$$\frac{1}{r}\frac{d}{dr}\left(r\lambda_C\frac{dT_C(r)}{dr}\right)=0$$

To solve ordinary differential equations, we need boundary conditions:

- Finite temperature at $r=0$
- 4^{th} kind b.c. at $r=r_{F0}$

$$T_F|_{r=r_{Fo}}=T_G|_{r=r_{Fo}}\quad \lambda_F\tfrac{dT_F}{dr}|_{r=r_{Fo}}=\lambda_G\tfrac{dT_G}{dr}|_{r=r_{Fo}} \tag{33}$$

- 4^{th} kind b.c. at $r=r_{Go}$

$$T_G|_{r=r_{Go}}=T_C|_{r=r_{Go}}\quad \lambda_G\tfrac{dT_G}{dr}|_{r=r_{Go}}=\lambda_C\tfrac{dT_C}{dr}|_{r=r_{Go}} \tag{34}$$

- 3^{rd} kind b.c. at $r=r_{Co}$

$$-\lambda_C\frac{dT_C}{dr}\bigg|_{r=r_{Co}}=h\left(T_{Co}-T_{lb}\right)$$

10.1 Thermal conductivity and heat transfer coefficient

In the single-phase regions, the Nusselt number, Nu, of the coolant was determined using the Dittus-Boelter equation [1] for heating

$$\mathrm{Nu_{DB}}=0.023\mathrm{Re}^{0.8}\mathrm{Pr}^{0.4} \tag{35}$$

where Pr is the Prandtl number [1].

$$\mathrm{Pr}=\frac{c_p\times\mu}{\lambda} \tag{36}$$

where λ is the thermal conductivity of the material whilst μ is its viscosity.

The Nusselt number of the whole fuel bundle in the single-phase regions, $\mathrm{Nu_{bundle}}$ [1], was then calculated by

$$\mathrm{Nu_{bundle}}=\mathrm{Nu_{DB}}(1+0.91\mathrm{Re}^{-0.1}\mathrm{Pr}^{0.4}(1-2e^{-B})) \tag{37}$$

where the value of B for a square lattice [1] is given by

$$B=\frac{4}{\pi}\left(\frac{p}{D_r}\right)^2-1 \tag{38}$$

where p is the lattice pitch, and D_r is the outer fuel rod diameter.

Then the single-phase heat transfer coefficient of the coolant, h_{lo} can be calculated as shown below

$$h_{lo}=\frac{\mathrm{Nu_{bundle}}\times\lambda}{D_h} \tag{39}$$

The two-phase heat transfer coefficient, $h_{2\varphi}$, was determined using the Collier and Pulling correlation [2] for regions where boiling occurs

$$h_{2\varphi}=h_{lo}\left(6700\frac{q''}{G\times i_{fg}}+2.34{\mathrm{X_{tt}}}^{-2}\right) \tag{40}$$

where $\mathrm{X_{tt}}$ is the Martinelli parameter [2].

$$\mathrm{X_{tt}}=\left(\frac{1-x}{x}\right)^{0.9}\left(\frac{\rho_g}{\rho_f}\right)^{0.5}\left(\frac{\mu_f}{\mu_g}\right)^{0.1} \tag{41}$$

The expression for thermal conductivity of the fuel, λ_F, [1] where t = T/1000 and T is the temperature, and a fuel porosity of 5% is assumed to get

$$\lambda_F=\frac{100}{7.5408+17.692t+3.6142t^2}+\frac{6400}{t^{\frac{5}{2}}}e^{-\frac{16.35}{t}} \tag{42}$$

The NRC-approved AREVA report considers the RELAP5 (default) data adequate to represent the thermal conductivity, λ_C, of the M5 alloy material for cladding [5]. A correlation based on the interpolation of these data is given in Eq. (43) within the temperature range of $T\leq 2133K$

$$\lambda_C=8.6383e^{0.0007T} \tag{43}$$

Moreover, the thermal conductivity of the helium gas gap, λ_G,[10] is given below

$$\lambda_G=0.0476+0.362\times10^{-3}T-0.618\times10^{-7}T^2+0.718\times10^{-11}T^3 \tag{44}$$

10.2 Fuel pellet temperature

From b.c., we can solve Eq. (32) using integration, resulting in

$$\lambda_F \frac{dT_F(r)}{dr} = -\frac{1}{r}\int q'''(z)\cdot r\cdot dr = -\frac{q'''(z)\cdot r}{2} + \frac{C}{r}$$

To limit $T_{Fc} = T_F(0)$, the constant C must be equal to zero: $C = 0$, thus

$$\lambda_F \frac{dT_F(r)}{dr} = -\frac{q'''(z)\cdot r}{2}$$

After integration, the temperature rise in the fuel region is as follows:

$$\Delta T_F(z) \equiv T_F(0) - T_F(r_F) = T_{Fc} - T_{Fo} = \frac{q'''(z)\cdot r_{Fo}^2}{4\cdot\lambda_F}$$

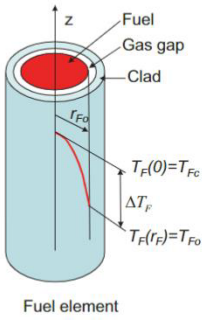

Figure 27: Typical cylindrical fuel element temperature distribution [1].

10.3 Cladding temperature

Since the conduction equation is the same in the clad region, the temperature rise in the clad is found as

$$\left.\begin{aligned} q''|_{r_{Go}} &= -\lambda_C \frac{dT_C(r)}{dr}\Big|_{r_{Go}} = -\frac{C'}{r_{Go}} \\ q''|_{r_{Go}}\cdot 2\pi r_{Go}\cdot dz &= q'''\cdot \pi r_{Fo}^2\cdot dz \end{aligned}\right\} \Rightarrow C' = -\frac{q'''r_{Fo}^2}{2} \tag{45}$$

Hence, we get

$$\Delta T_C = \frac{q'''r_{Fo}^2}{2\lambda_C}\ln[\frac{r_{Co}}{r_{Go}}]$$

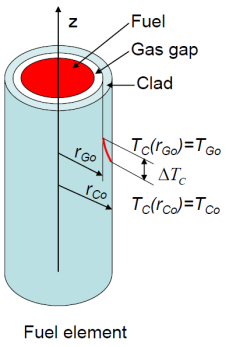

Figure 28: Typical cylindrical fuel element temperature distribution [1].

10.4 Fuel center-line temperature

The temperature at the center of the fuel, known as T_{Fc}, is calculated by adding the temperature of the coolant, T_{lb}, to the overall change in temperature of the fuel rod.

$$T_{Fc} = T_{lb} + \frac{q'}{4\pi}\left[\frac{1}{lambda_F} + \frac{2}{\lambda_G}\ln\left(\frac{r_{Go}}{r_{Fo}}\right) + \frac{2}{\lambda_C}\ln\frac{r_{Co}}{r_{Go}} + \frac{2}{r_{Co}h}\right] \tag{46}$$

Moreover, the outer fuel pellet temperature, T_{Fo}, is determined from the difference between the fuel center-line temperature and the temperature change in the fuel pellet. Consequently, the inner cladding temperature, T_{Ci}, is determined from the difference between the outer fuel pellet temperature and the temperature change in the gas gap, and it can be expressed as shown below

$$T_{Ci} = T_{Fo} - \frac{q'''r_{Fo}^2}{2\lambda_G}\ln\left(\frac{r_{Go}}{r_{Fo}}\right) \tag{47}$$

The maximum temperature will occur at the inner cladding surface, closest to the fuel.

10.5 Temperature distributions for clad and fuel pellet

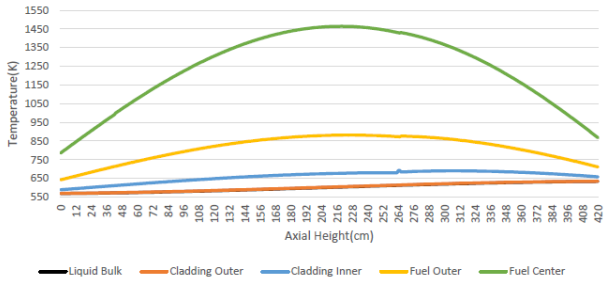

Figure 29: Axial temperature distribution for different parts of the cylinder fuel element.

Fig. 29 shows a slight jump in the cladding inner temperature at 264 cm due to introducing a two-phase flow. At this point, the heat transfer coefficient changes significantly, leading to a notable change in the shape of the temperature curves. Additionally, the cladding surface temperature is similar to the liquid bulk temperature, which is not visible in the above plot. Fig. 30 shows the radial temperature distribution.

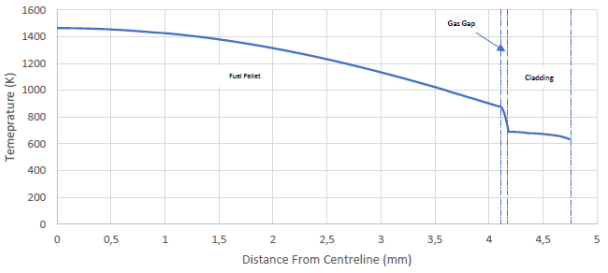

Figure 30: Radial temperature distribution for different parts of the cylinder fuel element.

11 Discussions and conclusion

The MS Excel macros module for XSteam developed under the guidelines of IAPWS (The International Association for the Properties of Water and Steam) [8] is used to perform this project's thermal-hydraulics calculations. However, there were some limitations in finding the values for dynamic viscosity for vapor or fluid phases. The input parameters in XSteam were perturbed a bit from its previous values to call for inlet values of viscosity and were assumed to be fluid. Conversely, the input parameter values to the next cell resulted in viscosity in the gas phase. Moreover, the parameters for plotting distributions are discretized axially into 101 nodes for specific calculations.

Based on the thermal-hydraulic calculations, it can be concluded that neither the cladding nor the fuel elements are in danger of melting hazards. The maximum fuel center temperature observed during the analyses was 1452 K, well below the melting point of UO2 and MOX fuels, about 3073 K and 3010 K for unirradiated elements, respectively. The maximum fuel outer temperature and the maximum cladding inner temperature were observed to be 858 K and 680 K, respectively. In comparison, the maximum cladding outer temperature and liquid bulk temperature were observed to be about 640 K. It is important to note that these values decrease with burn-up, indicating that the fuel geometry will be preserved during operation, and possible adverse effects of molten fuel on the cladding will be eliminated. During modes of operation associated with PCC1 and PCC2 events where PCC stands for plant condition category, there is at least a 95% probability that the peak linear power (in this case, 380 W/cm for hot channel and 220 W/cm for average channel), fuel rods will not exceed the fuel melting temperature at the 95% confidence level.

In conclusion, based on the calculations and findings presented in this report, it can be stated that there is at least a 95% probability at a 95% confidence level that departure from nucleate boiling (DNB) will not occur on the limiting fuel rods during normal operation and operational transients and in any transient conditions arising from faults of moderate frequency (PCC1 and PCC2 events). Therefore, neither the cladding nor the fuel elements are in danger of melting hazards.

References

[1] Henryk A. *Nuclear Reactor Technology and Design*. Springer International Publishing, 2019.

[2] Henryk Anglart. *Saturated Boiling, Dryout and Post-dryout Heat Transfer*. Stockholm: KTH Royal Institute of Technology, 2022.

[3] M Fischer and A Henning. "EPR engineered features for core melt mitigation in severe accidents". In: *Proceedings of ICAPP'09 paper 9061*. 2009.

[4] P. Kudinov. *SH2702 Project work description*. Technical report. Stockholm, Sweden, 2023.

[5] D. B. Mitchel and et al. *Evaluation of Advanced Cladding and Structural Material (M5™) in PWR Reactor Fuel*. Technical report BAW-10227-A. Non-Proprietary Version. Framatome Cogema Fuels, 2000.

[6] Maciej S. and Rafal L. "Thermal-hydraulic calculations for a fuel assembly in a European Pressurized Reactor using the RELAP5 code". In: *NUKLEONIKA* 60.3 (2015), pp. 537–544. DOI: 10.1515/nuka-2015-0110.

[7] Thiago A. S., Jose R. M., and Giovanni L. S. "A Thermal Hydraulic Analysis in PWR Reactors with UO2 or (U-Th)O2 Fuel Rods employing a Simplified Code". In: *Agenda Brasileira do ISBN*. 2015. ISBN: 978-85-99141-07-6.

[8] The International Association for the Properties of Water and Steam. *Revised Release on the IAPWS Industrial Formulation 1997 for the Thermodynamic Properties of Water and Steam*. Technical Report. 49 pages. Lucerne, Switzerland: IAPWS, 2007. URL: http://www.iapws.org/relguide/IF97-Rev.pdf.

[9] *The Pre-Construction Safety Report (PCSR) for UK EPR*. EDF Energy. 2008. URL: http://www.epr-reactor.co.uk/scripts/ssmod/publigen/content/templates/show.asp?P=290&L=EN&id_cat=1.2.

[10] N. Vargaftik. *Temperature Dependence of Thermal Conductivity of Helium*. New York: Plenum Publishing Corp., 1976.

12 Appendix

Thank you for taking the time to review our report and providing valuable feedback. We appreciate your comments and have made the necessary improvements to enhance the clarity and completeness of our work.

- **Task1 (ILO1, ILO2):**Regarding the reactor vessel and its dimensions, we have added the relevant information in the appropriate section of the report. We have also included additional technical details and operating conditions for the pressurizer volume and other reactor coolant system components. As suggested, we have provided more technical information that discusses the balance of plants. We have also included a literature study to provide sources for the facts and technical details that we have presented in the report. Finally, per your suggestions, we have specified the sources for all the figures used in the report.

- **Task2 (ILO1, ILO2):**We appreciate your feedback on the missing references in the start-up, normal, and shutdown operations sections. We added them to the "section" headings, suggesting that the whole section is based on the reference. We are glad to hear that the report covers all the required topics and even includes additional information. We hope that the improved version of the report meets your expectations.

- **Task3 (ILO1, ILO2):**We have included the core meltdown frequency and large release frequency in the PRA analysis and the required values by law in the section discussing the general principles of reactor safety [9]. Additionally, we have provided more references for figures and statements throughout the report to allow readers to check the statements' validity.

- **Task4 (ILO3):**We also appreciate your comments on the presentation of our input data. We have improved our documentation by citing the relevant sources and indicating when a parameter is an engineering estimate. We extended

the description of the applied equations to cover the calculation of the inlet orifices pressure drop, pressure drop calculations in two-phase flow, and void fraction model. We also provided more detailed information on how the system was discretized axially, including the number of cells employed and how the equations for pressure drop were discretized. We acknowledged the errors in our flow characteristics plot and investigated them further with improved results from our new calculations. Regarding our results, we made our figures slightly larger to improve readability. We also clarified in our methodology if we employed a power distribution of a cosine shape, which altered the shapes of the enthalpy and temperature distributions. We also discussed the pressure drop mechanisms that impact the distribution, plotted the friction, local, and gravity pressure drops individually, and compared our temperature distribution with literature values for inlet and outlet temperature.

- **Task5 (ILO4a):**We have added more context and discussion around the main/critical factors in each result and whether their behavior is expected. We have noted where each value in the collected data comes from, either by citing the relevant source or mentioning that it is an engineering estimate. We have extended the description of the applied equations, including the calculation of the inlet orifices pressure drop and pressure drop calculations in two-phase flow; the void fraction model distribution is exempted in our case as we are dealing with PWR but for the hot channel possibility of two-phase flow is taken into consideration by the usage of mixture density and viscosity, i.e., ρ_m and μ_m respectively, and the axial discretization of the system. We have also clarified the number of cells employed and how the equations were discretized for pressure drop. We have increased the size of the figures for better readability and added more discussion around the plotted power distribution, enthalpy and temperature distributions, and flow characteristics. We have addressed the issue with the hot channel's two-phase flow and included comments on the maximal power possible without reaching the two-phase flow, as well as what DNBR at the specific location would mean (a corrected value from the previous report is added). We have defined how the hot channel parameters depend on the peaking factor and have included more information on the Reddy-Fighetti correlations, which was used as it resembles most of the parameters we used for our EPR design (in our case, we studied UK EPR), as well as which one was applied to obtain the plot. We have also added more comments on the applicability ranges of each correlation and how our actual values compare to them by referring them to Tab. 3.

- **Task6 (ILO4b):**The thermal conductivity and heat transfer coefficients used in the calculations have been clarified in the report, along with details on how they were obtained. Different correlations to get the heat transfer coefficient have also been included. The report has been updated to discuss how the distributions for implementing the equations are shown in radial and axial profiles. The report has been revised to discuss how they found maximal temperatures correspond to the melting temperature of the fuel material and the maximum allowed value for the clad material.

Peer Reviews:

For peer review of the draft report, view them on the following pages.

Review of the Project Group:
Group Code: EPR41
Full title: General Features and Principles of EPR Nuclear Reactor Operation: A Design and Calculation Study

Intended learning outcome (ILO)	Grade (0-3)	The explanation for the grading of the evidence of achieving respective ILO. Suggestions for improvements and other comments
1. *Collect information on* the General design specification of the nuclear power plant with selected reactor type (Task 1, ILO1, ILO2)	**3**	*General reactor core description: covered in the report. Reactor vessel: covered in the report. Primary/secondary loop: covered in the report. Balance of plant: covered in the report. Most corrections were stylistic errors.
2. *Describe* the Operational principles of the power plant. (Task 2, ILO1, ILO2)	**3**	How is the reactor run during start-up, normal, and shutdown? Both base and load-following scenarios: Everything is covered in the report.
3. *Explain* the Safety features of the power plant. (Task 3, ILO1, ILO2)	**2**	General principles of reactor safety + key parameters: It'd be nice to see the core meltdown frequency and large release frequency from the PRA, if available, along with the required values by law.
4. *Calculate* Selected core parameters (Task 4, ILO3)	**2**	The results presentation needs to be improved, and some context is given. There is a lack of discussion about the main/key factors in each result and if their behavior is what we expect to see.
5. *Calculate* CHF margins in a hot channel (Task 5, ILO4a)	**2**	Again, the results are shown, but there is no discussion/commentary about them. It is difficult to conclude whether the learning outcome was fulfilled or not.
6. *Calculate* Maximum cladding and fuel pellet temperature (Task 6, ILO4b)	**1**	Like Tasks 4 and 5. Additionally, there is no information about the thermal conductivity nor a graph showing the temperature change across the fuel pellet.

*The report itself was commented on to suggest improvements and corrections.

Review of the Project Group:
Group Code: 41 EPR
Full title: General Features and Principles of EPR Nuclear Reactor Operation: A Design and Calculation Study

It was sometimes unclear which section corresponded to which Task, so for the final report it could be helpful to structure it more aligned to the prompted tasks. For all tasks, I included more detailed comments in the pdf directly.

Intended learning outcome (ILO)	Grade (0-3)	Explanation for the grading of the evidences of achieving respective ILO. Suggestions for improvements and other comments
1. *Collect information on* General design specification of the nuclear power plant with selected reactor type (Task 1, ILO1, ILO2)	2	The description of the reactor core is very detailed. The section about the reactor coolant system and its components is supported by helpful figures. Only at some points more information could be included, such as the dimensions, the operating and design conditions of the vessel or the pressurizer volume (commented in the text). The plant layout, which is not necessarily required in the task (unless it is presented as being unique for the EPR design) and thus additional information. The secondary loop and the balance of plant is not described as an independent section. Some relevant information is in section 2.1 Plant Layout. However, it only mentions the location of different balance of plant components. More technical information on the turbine, condenser, feedwater-cycle could be included. Task 1 should include a literature study, yet no reference was provided during the text. When facts and technical details are defined, the corresponding sources would be important for verification. For figures, unless they were really created by the authors themselves, the source must be specified.
2. *Describe* Operational principles of the power plant. (Task 2, ILO1, ILO2)	2	The report discusses reactor shutdown, draining and opening of the primary system, core un- and reloading, closing and filling of the primary system, as well as heating of the primary coolant. Then it continues discussing which operations are necessary to achieve power operation after a cold shutdown, and describing normal operation and load-following. It includes additional information on extended cycle operation as well as preventive maintenance. Methods for reactivity control are described as well. Thus, the description covers all required topics and even includes additional information. Unfortunately, as before, the references are again missing in this section. Possibly, the same reference was used for the complete report – if so, that should be indicated somewhere.

3. *Explain* Safety features of the power plant. (Task 3, ILO1, ILO2)	2	The safety systems are discussed starting in section 3. Various safety systems of the EPR are described there. Further discussion of Nuclear Safety is provided in section 6 on Nuclear Safety. In this section, the principles of reactor safety are discussed. Unfortunately, the results of reactor safety analysis and some key safety parameters, such as, e.g., core damage frequency are missing. As in the above tasks, references were missing for figures and statements. Including sources at the end of each paragraph and for each figure would allow the reader to find more information and check the validity of the statements made.
4. *Calculate* Selected core parameters (Task 4, ILO3)	1	Input data has been collected. The presentation of the collected data could be improved by noting, where each value comes from. This could be done by either citing the relevant source or mentioning that a parameter is an engineering estimate. The description of the applied equations could be improved by extending it for the calculation of the inlet orifices pressure drop, pressure drop calculations in two phase flow, void fraction model, etc. Also, it should be clarified in more detail, how the system was discretized axially, particularly by including how many cells were employed and how the equations such as for pressure drop were discretized. The results are provided as figures only. Readability could be improved if the figures were a bit larger. The plotted power distribution differs from the expected cosine shape, which also alters the shapes of the enthalpy and temperature distributions. If a power distribution different from a cosine-shape was employed, it should be mentioned in the methodology. The flow characteristics indicate errors in the calculation, as the pressure drop found for nominal conditions ~0.3 MPa differs significantly from the pressure drop at 100% power and 100% flow ~0.1 MPa in the flow characteristics plot. The plots are neither described nor discussed. Possible ideas for discussion are: - Which pressure drop mechanisms have the largest impact on the pressure drop distribution in (a)? The friction, local, gravity pressure drops could be plotted individually to support possible comments. - Does the obtained temperature distribution agree with literature values for in- and outlet temperature? - What is the reason that the flow characteristics differ so much for high and low flow rates? Why is the pressure drop in the heated cases smaller than in the non-heated case when approaching zero flow rate? Which pressure drop mechanisms are most relevant at different flow rates?
5. *Calculate* CHF margins in a hot channel (Task 5, ILO4a)	1	The peaking factor is discussed in detail in section 8.3 for critical heat flux. It could be improved by defining how the hot channel parameters depend on the peaking factor. The Bowring

		correlation and the Reddy-Fighetti correlations are introduced. It is unclear, which of them was applied to obtain Figure 16 (e) and (f). Further comments on the applicability ranges of each correlation and how your actual values compare to them should be made. Again, the resulting plots are not described. The plots would be better visible if they were a little larger. Legends for plots including more than one curve (average and hot channel) should be included. In Figure 16 (c) it seems like two-phase-flow is reached in the hot channel, which should not happen in a PWR design. Therefore, comments on this should be included. Particularly the maximal power possible without reaching two phase flow should be reported as discussed in the lecture. Further discussion could cover what a DNBR of 1.71 at a location of 350 cm would mean.
6. *Calculate* Maximum cladding and fuel pellet temperature (Task 6, ILO4b)	1	Heat conduction calculations in the fuel, gap and cladding are described. It is not mentioned how the thermal conductivities and the heat transfer coefficients were obtained. The task stated that temperature dependent thermal conductivities of clad and fuel materials should be assumed. Further, since two phase flow was reached in the hot channel, different correlations to obtain the heat transfer coefficient are necessary. Finally, the report could be extended by explaining how these equations were implemented in the code, i.e., was the system discretized radially, or were there iterations to find the cladding average temperature for the cladding thermal conductivity? The axial temperature profiles for outer fuel and fuel center, as well as for outer and inner cladding are provided as plots. In addition, the maximal temperatures, and locations in each of these profiles are noted. The report could be improved by discussing how the found maximal temperatures correspond to the melting temperature of the fuel material and the maximum allowed value for the clad material.